PHYSICAL REVIEW FLUIDS **2**, 092602(R) (2017)

Hysteretic transitions between quasi-two-dimensional flow and three-dimensional flow in forced rotating turbulence

Naoto Yokoyama*
Department of Aeronautics and Astronautics, Kyoto University, Kyoto 615-8540, Japan

Masanori Takaoka†
Department of Mechanical Engineering, Doshisha University, Kyotanabe 610-0394, Japan
(Received 30 January 2017; published 27 September 2017)

Conflict between formation of a cyclonic vortex and isotropization in forced homogeneous rotating turbulence is numerically investigated. It is well known that a large rotation rate of the system induces columnar vortices to result in quasi-two-dimensional (Q2D) flow, while a small rotation rate allows turbulence to be three-dimensional (3D). It is found that the transition from the Q2D turbulent flow to the 3D turbulent flow and the reverse transition occur at different values of the rotation rates. At intermediate rotation rates, bistability of these two statistically steady states is observed. Such a hysteretic transition is also observed for variations of the amplitude of an external force.

DOI: 10.1103/PhysRevFluids.2.092602

Formation of columnar structures parallel to a rotation axis is one of the most fundamental and distinctive phenomena in flows subject to rotation. The emergence of columnar vortices in the rotating turbulence makes a three-dimensional (3D) flow into a quasi-two-dimensional (Q2D) flow. The Taylor-Proudman theorem has succeeded in explaining the cylindrical flow in laboratory experiments and field observations in terms of the Taylor column. However, the theorem cannot describe transitions between the Q2D and 3D flows, because energy is exchanged between the Q2D mode and the 3D mode by nonlinear mechanisms [1]. The energy transfers to the Q2D modes were demonstrated by an instability analysis [2] and the weak-turbulence theory in the large-rotation limit [3]. The Coriolis term breaks the parity invariance of the governing equation of the flow, and introduces a scale-independent time scale which induces two-dimensionalization at larger scales more effectively. Therefore, the Coriolis effect originates cyclone-anticyclone asymmetry with enhanced stretching of cyclonic vorticity and destabilization of the anticyclonic vortex due to centrifugal instability and vortex tilting [4].

To classify the flow properties in rotating systems, the Rossby number Ro, which is the ratio between linear and nonlinear time scales, has been used [5]. Note that though various definitions of Ro are used in literature, the following facts are independent of its detailed definition. When the Coriolis force is weak relative to turbulence, i.e., $\mathrm{Ro} \gg 1$, the 3D Kolmogorov turbulence is obtained. When $\mathrm{Ro} \sim 1$, only cyclonic vortices appear at large scales, and the flow becomes Q2D. When $\mathrm{Ro} \ll 1$, both cyclonic and anticyclonic vortices appear, and the flow fields are almost completely two-dimensionalized. The transitions between the Q2D turbulence and the 3D turbulence by changing the system's rotation rate Ω were numerically studied [6]. It was reported that the Ro dependence of turbulent statistics is not monotonic in the range $\mathrm{Ro} \sim 1$, where the coherent vortices and inertial waves at small wave numbers and the turbulence at large wave numbers coexist [7,8]. The two-dimensionalization and the cyclone-anticyclone asymmetry depend on the external forces and the boundary conditions (e.g., Ref. [9]).

*yokoyama@kuaero.kyoto-u.ac.jp
†mtakaoka@mail.doshisha.ac.jp

Recently, Ref. [10] reported a phase diagram for statistically steady states of forced Taylor-Green (TG) flows in a rotating frame. Four different steady states in the parameter space spanned by the Reynolds numbers and the Rossby numbers were numerically obtained by carrying out 184 simulations. Subcritical behavior was implied by an abrupt transition between the Q2D and 3D flows. If it were a low-dimensional system, one might expect a hysteresis in such a transition. Because the parameter space analysis was performed with the same random initial condition for every parameter value in Ref. [10], the hysteretic behavior cannot be directly found.

It has been experimentally found that there exists a parameter range where a high-torque state and a low-torque state are bistable and show a hysteretic transition in a highly turbulent Taylor-Couette flow [11]. A similar hysteretic transition was observed also in rotating spherical Couette flow [12]. Bistability and hysteresis between a stationary magnetic field and an oscillatory magnetic field in a low-dimensional phase space were observed in a turbulent flow of liquid sodium [13]. Note that the heteroclinic alternating transitions such as blocking in a rotating annulus [14] associated with the Lorenz attractor, where the state goes back and forth near the two *unstable* fixed points, are different from the bistability. Also note that the bistability does not necessarily indicate a hysteresis, which requires a form of subcritical properties. The dynamical systems theory developed in low-dimensional systems has successfully been applied to the onset of turbulence, e.g., unstable periodic orbits in wall turbulence [15]. The bifurcation structures embedded in developed turbulence would be a key to understanding its nature.

Hysteretic behavior in developed turbulence has mostly been observed in the flows bounded by solid walls, and the boundary condition plays an important role in the hysteretic behavior. In this Rapid Communication, a hysteretic behavior in developed rotating turbulence is numerically investigated in a periodic box. As far as the authors are aware, such behavior in the system not bounded by the solid walls has rarely been reported. While the boundary condition and the forcing scheme in the present study are the same as those in Ref. [10], the analytical methodologies for the parameter dependence of the flow patterns are different; a flow field in the statistically steady state for a close parameter is employed as an initial condition in this study, whereas a random initial condition was used in Ref. [10]. The present approach is similar to the continuation of a solution which enables us to track a branch in multistability used in bifurcation analysis in low-dimensional dynamical systems.

We examine the dependence of flow properties on Ω as well as the amplitude of the external force, focusing on the transition between the Q2D flow and the 3D flow. The micro-Rossby number defined below as well as the Taylor-scale Reynolds number is usually employed as the nondimensional parameter to characterize the flow field. However, it is statistically defined by the flow itself, and cannot be a control parameter. The macro-Rossby number and the integral-scale Reynolds number can be used as control parameters, but they do not well characterize the turbulent field. As we will see below, the transitions are hysteretic owing to the robustness of the large-scale columnar vortex against the turbulent fluctuation.

The governing equations for the velocity $\boldsymbol{u}$ of the incompressible fluid are the Navier-Stokes equation with the Coriolis term and the divergence-free condition,

$$\frac{\partial \boldsymbol{u}}{\partial t} + (\boldsymbol{u}\cdot\nabla)\boldsymbol{u} + 2\boldsymbol{\Omega}\times\boldsymbol{u} = -\nabla p + \nu\nabla^2\boldsymbol{u} + \boldsymbol{f}, \quad \nabla\cdot\boldsymbol{u} = 0,$$

where the centrifugal force is included in the pressure p. The rotation vector $\boldsymbol{\Omega} = \Omega\boldsymbol{e}_z$ is assumed to be constant. The kinematic viscosity is expressed by ν. Note that small-wave-number drag is not added, because it was reported that a statistically steady state can be achieved even for the inversely cascading two-dimensional turbulence [16]. The external force $\boldsymbol{f}$ is given by the three-dimensional two-component force of a steady TG type $\boldsymbol{f} = f_0(\cos k_\mathrm{f} x \sin k_\mathrm{f} y \sin k_\mathrm{f} z, -\sin k_\mathrm{f} x \cos k_\mathrm{f} y \sin k_\mathrm{f} z, 0)$, where $k_\mathrm{f} = 2$ is employed. The TG flow has also been used as a model of many laboratory flows (see Ref. [10]).

In the present simulations, the periodic boundary condition with the period $(2\pi)^3$ is employed. The standard pseudospectral method with the aliasing removal by the phase shift and the spherical truncation is adopted for the nonlinear term, and the numerical resolution is 512^3. The same value of

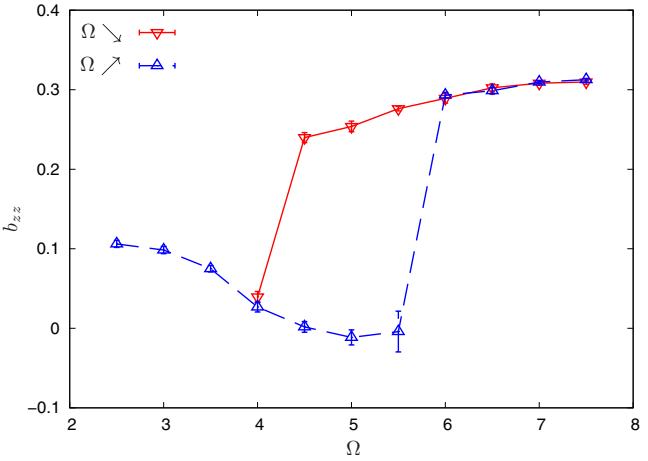

FIG. 1. Dependence of zz component of anisotropy tensor b_{zz} on Ω. The solid curve (Ω ↘) and the dashed curve (Ω ↗), respectively, show b_{zz} during the decrease of Ω and the increase of Ω. The error bars represent the standard deviation due to the time variation.

ν is used for all the series of the simulations. The Runge-Kutta-Gill method is adopted for the time integration, while the linear terms are calculated analytically. The characteristic length and time are selected so that the period of the computational box is 2π, and the Coriolis parameter 2Ω and the amplitudes of the external force f_0 are approximately 10.

Let us first consider Ω dependence. The rotation rate Ω is set between 2.5 and 7.5 by 0.5 increments or decrements, while f_0 is fixed at 10. The rotation rate is increased or decreased by 0.5 when the flow field for the previous rotation rate is in the statistically steady state. The Zeman wave numbers $k_\Omega = (\Omega^3/\varepsilon)^{1/2}$, where ε is the energy dissipation rate, are evaluated approximately as 1.4 for $\Omega = 2.5$ and 16 for $\Omega = 7.5$. The corresponding flows are 3D and Q2D.

Since we are interested in the transitions between the Q2D turbulent flow and the 3D turbulent flow, the dependence of the zz component of the anisotropy tensor, $b_{zz} = 1/3 - \langle u_z^2\rangle/\langle|\boldsymbol{u}|^2\rangle$, on Ω is drawn in Fig. 1 to evaluate the anisotropy of the flows. These values are obtained in the statistically steady states.

At $\Omega = 2.5$, $b_{zz} \approx 0.1$, where the nonzero value comes from the anisotropic external force of the TG type. When the rotation rate is increased from $\Omega = 2.5$ (Ω ↗), b_{zz} decreases to almost 0, where the flow is 3D and almost isotropic. It increases abruptly to about 0.3 in the range of $5.5 < \Omega < 6$, and the flow becomes Q2D and strongly anisotropic. At $\Omega = 7.5$, $b_{zz} \approx 0.3$ owing to the strong rotation. When the rotation rate is decreased from $\Omega = 7.5$ (Ω ↘), b_{zz} slowly decreases. In the range of $4 < \Omega < 4.5$, b_{zz} drops sharply, representing the abrupt transition from the Q2D anisotropic flow to the 3D isotropic flow. In the range of $4.5 \lessapprox \Omega \lessapprox 5.5$, the two turbulent regimes are bistable and show a hysteretic transition.

To characterize the upper- and lower-branch flows shown in Fig. 1, the Fourier- and real-space properties at $\Omega = 5$ are examined. The one-dimensional energy spectra are drawn in Fig. 2(a). For the lower-branch flow (Ω ↗), where $k_\Omega \approx 8.6$, the Kolmogorov spectrum $k^{-5/3}$ appears all over the inertial subrange. For the upper-branch flow (Ω ↘), while the Kolmogorov spectrum appears in the range $k \gtrapprox k_\Omega \approx 6.0$, the energy spectrum at $k \lessapprox k_\Omega$ shows another turbulent state. A significant difference between the upper- and lower-branch flows appears at the small wave numbers; while the largest energy of the former appears at the scale of the external force, $\sqrt{3}k_\mathrm{f} \approx 3.46$, that of the latter appears at the largest scale $k = 1$.

In the lower-branch flow, the energy supplied by the external force is almost completely transferred to the larger wave numbers as the 3D Kolmogorov turbulence. In the upper-branch flow, on the other

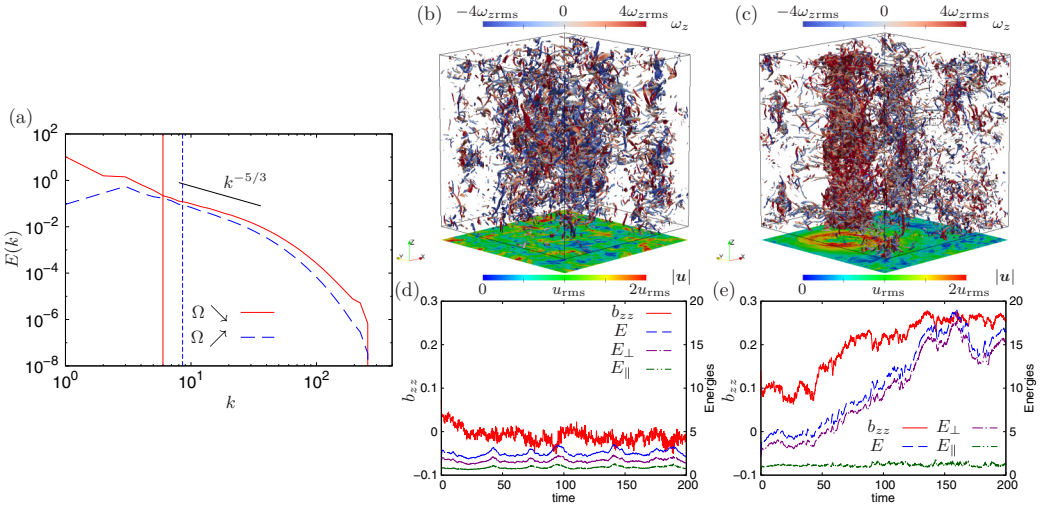

FIG. 2. Bistability between the Q2D flow and the 3D flow at $\Omega = 5$. (a) Energy spectra. The vertical lines represent the Zeman wave numbers. (b), (c) Isosurfaces of $|\boldsymbol{\omega}| = \pm 3\sqrt{\langle |\boldsymbol{\omega}|^2 \rangle}$ colored by ω_z and speed distribution on the $z = 0$ plane (b) for lower branch $\Omega \nearrow$ and (c) for upper branch $\Omega \searrow$. (d), (e) Time evolution of b_{zz} (left axis) and total, perpendicular and parallel, energies (right axis) (d) for the interpolation weight $r = 0.2$ and (e) for $r = 0.3$ between the Q2D flow and the 3D flow.

hand, a part of the supplied energy is transferred to the smaller wave numbers owing to the quasi-two-dimensionalization, and the field reaches a statistically steady state when the accumulation at $k \approx 1$, more precisely, $(k_x, k_y, k_z) = (\pm 1, 0, 0), (0, \pm 1, 0)$, is built up. The process of the accumulation is known as condensation. The inverse cascade due to the quasi-two-dimensionalization and the forward cascade from the accumulation to the large wave numbers are considered to balance each other in the statistically steady state. Similar discussions can be found in Ref. [10].

The Q2D flow has a larger energy than the 3D flow over all the wave numbers. Therefore, the two turbulent flows have different values of the micro-Rossby number $\mathrm{Ro}_{\omega_z} = \omega_{z\mathrm{rms}}/(2\Omega)$ as well as the Taylor-scale Reynolds number $\mathrm{Re}_\lambda = [20E^2/(3\nu\varepsilon)]^{1/2}$ under the identical values of the parameters of the simulations: $\mathrm{Ro}_{\omega_z} \approx 2.5$ and $\mathrm{Re}_\lambda \approx 490$ in the Q2D flow, and $\mathrm{Ro}_{\omega_z} \approx 1.8$ and $\mathrm{Re}_\lambda \approx 110$ in the 3D flow. Here, the subscript rms denotes the root mean square, and E is the total energy. Note that the Taylor microscale for the isotropic turbulence is used to obtain the values of Re_λ, because the Kolmogorov spectrum appears at the large wave numbers in both Q2D and 3D flows. The fact that Ro_{ω_z} in the Q2D flow is larger than that in the 3D flow causes the nonmonotonicity of the Ro dependence of turbulent statistics, as reported in Ref. [7].

The isosurfaces of vorticity norm $|\boldsymbol{\omega}|$ in the real space are drawn in Figs. 2(b) and 2(c). In the lower-branch flow, Fig. 2(b), no large-scale vortex is formed, and we can observe only small-scale 3D vortices. On the other hand, in the upper-branch flow, Fig. 2(c), the isosurfaces show the cyclonic vortex aligned along the rotation axis, which reminds us of the Taylor column. The cyclonic vortex makes strongly sheared regions between itself and its images due to the periodic boundary condition. In the strongly sheared regions, a cylindrical swarm composed of anticyclonic small-scale vortices is produced, though they are weak. In fact, the cyclonic vortex makes a high-speed whirl, as drawn on the $z = 0$ plane in Fig. 2(c), while the swarm does not. The cyclonic vortex accompanied by inertial waves makes the upper-branch flow Q2D.

Even though the simulations were run for a long time, the possibility of transitions between the Q2D flow and the 3D flow cannot be excluded. To confirm bistability at $\Omega = 5$, the existence of a basin of attraction of the Q2D flow and the 3D flow is examined by starting from interpolated initial conditions. The initial conditions are made by the superposition of the Q2D flow and the 3D flow

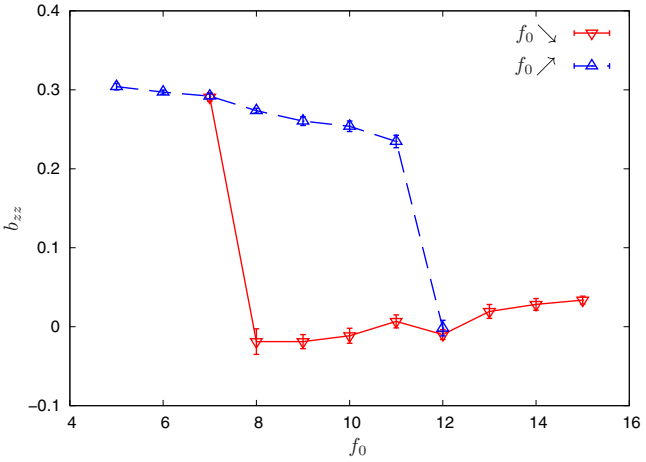

FIG. 3. f_0 dependence of b_{zz}. See also the caption of Fig. 1.

$\boldsymbol{u} = r\boldsymbol{u}_{\mathrm{Q2D}} + (1-r)\boldsymbol{u}_{\mathrm{3D}}$, where $r \in [0,1]$ is the weight for the interpolation between the Q2D flow and the 3D flow. The simulations are performed for the weights $r = 0.1, 0.2, \ldots, 0.9$ until each field reaches a statistically steady state.

The time evolutions of b_{zz}, E, perpendicular energy $E_\perp = \sum_{\boldsymbol{k}} |\widetilde{\boldsymbol{u}}_\perp|^2/2$, and parallel energy $E_\parallel = \sum_{\boldsymbol{k}} |\widetilde{u}_z|^2/2$ for $r = 0.2$ and 0.3 are drawn in Figs. 2(d) and 2(e). Here, $\widetilde{\boldsymbol{u}}_\perp$ is the Fourier coefficient of the velocity component perpendicular to the rotation axis $\boldsymbol{u}_\perp = (u_x, u_y, 0)$. In the simulation with $r = 0.2$, b_{zz} decreases to around 0, while b_{zz} increases to around 0.25 in the simulation with $r = 0.3$. That is, the boundary separating the Q2D flow and the 3D flow exists in the range $0.2 < r < 0.3$, and the Q2D flow and the 3D flow are bistable at $\Omega = 5$. The separatrix might not be a thin boundary such as the one which separates laminar and turbulent flows at the onset of turbulence [17] but a thick and blurred region.

It is of interest to note that both $E_\parallel$'s for $r = 0.2$ and 0.3 remain small and the main difference appears in $E_\perp$. Since $b_{zz} = 1/3 - E_\parallel/(E_\perp + E_\parallel)$, the transitions between the Q2D flow and the 3D flow occur mainly in $\boldsymbol{u}_\perp$, i.e., ω_z. In other words, the fluctuation in the rotation direction u_z is little affected by the rotation.

At the transition from the 3D flow to the Q2D flow, the coherent cyclonic vortex is formed by overwhelming the external force as well as turbulent fluctuation. The external force in the present simulations tries to develop the TG vortices whose symmetries and scales are different from the coherent cyclonic vortex. On the other hand, at the reverse transition, the coherent vortex collapses into pieces. The formation and destruction of the large coherent vortex cannot be continuous for the variation of Ω. Therefore, the transitions exhibit hysteresis.

The dependence of b_{zz} on the amplitude of the external force f_0, which is increased by increments of 1 or decreased by decrements of 1, is drawn in Fig. 3. Following the results of the Ω dependence in Fig. 1, we here investigate the cases with $\Omega = 5$ as the representative cases. Similar to Fig. 1, the Q2D flow and the 3D flow are, respectively, observed at small f_0 and large f_0, and the two turbulent flows are bistable and hysteretic at intermediate f_0. Obviously, this two-dimensionalization is due to the cyclonic vortex along the rotation axis.

To analyze the properties of the above hysteretic transition at the large and small scales, the dependences of the total energy E and the energy dissipation rate ε on Ω and f_0 are shown in Fig. 4. These figures show different behaviors between the Ω and f_0 dependences even qualitatively. The transitions of E and ε show the bistability in $4.5 \lessapprox \Omega \lessapprox 5.5$ and $8 \lessapprox f_0 \lessapprox 11$, as observed in Figs. 1 and 3. However, both E and ε have different values at large Ω where the flow is Q2D. No clear jump in $5.5 \leqslant \Omega \leqslant 6$ can be seen in ε for increasing Ω in Fig. 4(a). In other words, small-scale dynamics

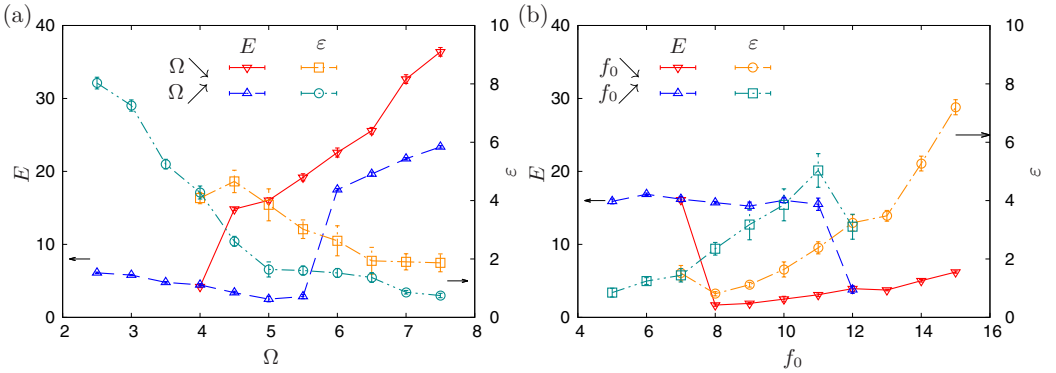

FIG. 4. (a) Ω dependence and (b) f_0 dependence of total energy (left axis) and energy dissipation rate (right axis).

is insensitive to Ω, which is consistent with the fluctuation in the rotation direction $E_\parallel$ observed in Figs. 2(d) and 2(e).

The fact that the discrepancy between the two branches at large Ω is larger than the turbulent fluctuation and the hysteresis loop is not closed implies the multiplicity of the statistically steady states of the Q2D flows. The multiplicity is confirmed by finding the separatrix of the superposition of the two flows in the same way that we demonstrated the bistability between the Q2D flow and the 3D flow at $\Omega = 5$ [Figs. 2(d) and 2(e)]. It should be noted that b_{zz} shown in Fig. 1, which is a nondimensionalized quantity composed of the ratio of the parallel energy to the total one, is insensitive to the variation of the energies themselves.

It may appear to be counterintuitive that the total energy for the small external force is larger than that for the large external force, as shown in Fig. 4(b). It can be explained by the formation process of the large-scale cyclonic vortex. When the external force is weak, the Coriolis force is strong relative to the turbulence intensity. Then, the large-scale columnar vortex is formed, and it makes the large energy accumulation near $k_z = 0$. Conversely, when the external force is strong, the Coriolis force is relatively weak. Then, the turbulent flow is 3D, and all the energy supplied by the external force is cascaded forward. As a result, the energy does not accumulate near $k_z = 0$, and the total energy is small.

Lastly, to investigate the characteristics of the multiplicity at large Ω's appearing in Fig. 4(a), the isosurfaces of $|\boldsymbol{\omega}|$ for each branch at $\Omega = 7.5$ are shown in Fig. 5(a). Obviously, both flows

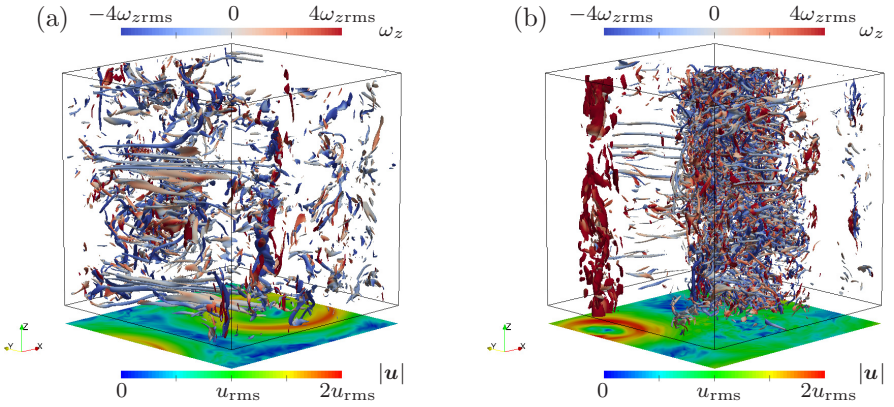

FIG. 5. Isosurface of $|\boldsymbol{\omega}| = \pm 3\sqrt{\langle |\boldsymbol{\omega}|^2 \rangle}$ colored by ω_z and speed distribution on the $z = 0$ plane at $\Omega = 7.5$. (a) Lower branch, and (b) upper branch.

have the Q2D structures as indicated in Fig. 1. While the upper-branch flow has the strong slender cyclonic vortex accompanied by a swarm of anticyclonic small vortices, the cyclonic vortex in the lower-branch flow is relatively weak and fat, and there is no room for the anticyclonic swarm to grow. These flow patterns as well as the total energy and the energy dissipation rate reveal the distinctive features degenerated in the representation in terms of b_{zz}. The Q2D flow might have more multiplicities other than those shown here.

Comparing with the phase diagram in Ref. [10], we recognize that most of the parameter values in the present study fall into the quasi-2D condensates, while some are located narrowly in the range of intermittent bursts and weakly rotating flows. The quasi-2D condensates and the weakly rotating flows in Ref. [10], respectively, correspond to the Q2D flow and the 3D flow reported here. An abrupt change in energy due to a variation of the Rossby number between the Q2D flow and the 3D flow was observed, and subcritical behavior was implied by the abrupt change. It should, however, be noted that the initial conditions used in Ref. [10] were not the solutions for other parameters. In this Rapid Communication, the Q2D and 3D branches were traced by continuing the solution to find whether the subcritical behavior results in the hysteretic transition or the heteroclinic alternating transitions in large turbulent fluctuations. The intermittent bursts are not observed in this study, but intermittent growths of the total energy which are caused by energy transfers to small wave numbers for a short time appear in the 3D flow, as recognized in Fig. 2(d). The intermittent growths in the 3D flow are more frequent and not so strong as the intermittent bursts observed in Ref. [10].

In summary, the Ω dependence and the f_0 dependence of turbulent flows were investigated by numerically simulating the Navier-Stokes equation with the Coriolis term under steady forcing of the TG type. The hysteretic transition between the Q2D flow at large Ω's and the 3D flow at small Ω's was found. This hysteretic transition stems from the robustness of the large-scale cyclonic columnar vortex. The hysteretic transition between the Q2D flow and the 3D flow exists for a finite bounded area in (Ω, f_0). Although the flow properties had been classified simply by using the micro-Rossby number [7] and summarized in a phase diagram in Ref. [10], the present results demonstrate that the selection of flow structures depends also on the initial conditions. The hysteresis brings the complexity of Ro dependence at $\mathrm{Ro} \sim 1$.

This hysteretic transition robustly exists against the large fluctuation of the fully developed turbulence whose energy spectra show the $-5/3$ power law. We also performed preliminary simulations in which flows are excited by a white random force [18]. The hysteresis and the bistability between the Q2D turbulent flow and the 3D turbulent flow are observed also for such antithetical forcing, though the range of the bistable parameters is much smaller. The existence of a universal mechanism for the emergence of multiple flow patterns in turbulence is expected. The dependence of hysteretic behavior on forcing types, the multiplicity of the Q2D flow, and the formation mechanism of the hysteretic behavior will be reported elsewhere.

Numerical computation in this work was carried out at the Yukawa Institute Computer Facility, Kyoto University and Research Institute for Information Technology, Kyushu University. This work was partially supported by JSPS KAKENHI Grants No. 15K17971 and No. 16K05490.

[1] F. Bellet, F. S. Godeferd, J. F. Scott, and C. Cambon, Wave turbulence in rapidly rotating flows, J. Fluid Mech. **562**, 83 (2006).

[2] F. Waleffe, The nature of triad interactions in homogeneous turbulence, Phys. Fluids A **4**, 350 (1992); Inertial transfers in the helical decomposition, *ibid.* **5**, 677 (1993); L. M. Smith and F. Waleffe, Transfer of energy to two-dimensional large scales in forced, rotating three-dimensional turbulence, *ibid.* **11**, 1608 (1999).

[3] S. Galtier, Weak inertial-wave turbulence theory, Phys. Rev. E **68**, 015301 (2003).

[4] P. Bartello, O. Métais, and M. Lesieur, Coherent structures in rotating three-dimensional turbulence, J. Fluid Mech. **273**, 1 (1994); C. Cambon, J.-P. Benoit, L. Shao, and L. Jacquin, Stability analysis and

large-eddy simulation of rotating turbulence with organized eddies, *ibid.* **278**, 175 (1994); B. Sreenivasan and P. A. Davidson, On the formation of cyclones and anticyclones in a rotating fluid, Phys. Fluids **20**, 085104 (2008).

[5] E. J. Hopfinger, F. K. Browand, and Y. Gagne, Turbulence and waves in a rotating tank, J. Fluid Mech. **125**, 505 (1982); J. Bardina, J. H. Ferziger, and R. S. Rogallo, Effect of rotation of isotropic turbulence: Computation and modeling, *ibid.* **154**, 321 (1985); P. K. Yeung and Y. Zhou, Numerical study of rotating turbulence with external forcing, Phys. Fluids **10**, 2895 (1998).

[6] L. M. Smith, J. R. Chasnov, and F. Waleffe, Crossover from Two- to Three-Dimensional Turbulence, Phys. Rev. Lett. **77**, 2467 (1996); E. Deusebio, G. Boffetta, E. Lindborg, and S. Musacchio, Dimensional transition in rotating turbulence, Phys. Rev. E **90**, 023005 (2014).

[7] L. Bourouiba and P. Bartello, The intermediate Rossby number range and two-dimensional–three-dimensional transfers in rotating decaying homogeneous turbulence, J. Fluid Mech. **587**, 139 (2007).

[8] A. Campagne, B. Gallet, F. Moisy, and P.-P. Cortet, Disentangling inertial waves from eddy turbulence in a forced rotating-turbulence experiment, Phys. Rev. E **91**, 043016 (2015).

[9] F. S. Godeferd and F. Moisy, Structure and dynamics of rotating turbulence: A review of recent experimental and numerical results, Appl. Mech. Rev. **67**, 030802 (2015).

[10] A. Alexakis, Rotating Taylor-Green flow, J. Fluid Mech. **769**, 46 (2015).

[11] S. G. Huisman, R. C. A. van der Veen, C. Sun, and D. Lohse, Multiple states in highly turbulent Taylor-Couette flow, Nat. Commun. **5**, 3820 (2014); S. Grossmann, D. Lohse, and C. Sun, High-Reynolds number Taylor-Couette turbulence, Annu. Rev. Fluid Mech. **48**, 53 (2016); R. C. A. van der Veen, S. G. Huisman, O.-Y. Dung, H. L. Tang, C. Sun, and D. Lohse, Exploring the phase space of multiple states in highly turbulent Taylor–Couette flow, Phys. Rev. Fluids **1**, 024401 (2016).

[12] D. S. Zimmerman, S. A. Triana, and D. P. Lathrop, Bi-stability in turbulent, rotating spherical Couette flow, Phys. Fluids **23**, 065104 (2011).

[13] M. Berhanu, B. Gallet, R. Monchaux, M. Bourgoin, Ph. Odier, J.-F. Pinton, N. Plihon, R. Volk, S. Fauve, N. Mordant, F. Pétrélis, S. Aumaître, A. Chiffaudel, F. Daviaud, B. Dubrulle, and F. Ravelet, Bistability between a stationary and an oscillatory dynamo in a turbulent flow of liquid sodium, J. Fluid Mech. **641**, 217 (2009).

[14] E. R. Weeks, Y. Tian, J. S. Urbach, K. Ide, H. L. Swinney, and M. Ghil, Transitions between blocked and zonal flows in a rotating annulus with topography, Science **278**, 1598 (1997).

[15] G. Kawahara and S. Kida, Periodic motion embedded in plane Couette turbulence: Regeneration cycle and burst, J. Fluid Mech. **449**, 291 (2001).

[16] C.-K. Chan, D. Mitra, and A. Brandenburg, Dynamics of saturated energy condensation in two-dimensional turbulence, Phys. Rev. E **85**, 036315 (2012).

[17] T. Itano and S. Toh, The dynamics of bursting process in wall turbulence, J. Phys. Soc. Jpn. **70**, 703 (2001); T. M. Schneider and B. Eckhardt, Edge states intermediate between laminar and turbulent dynamics in pipe flow, Phil. Trans. R. Soc. A **367**, 577 (2009).

[18] See Supplemental Material at http://link.aps.org/supplemental/10.1103/PhysRevFluids.2.092602 for hysteresis and bistability in rotating turbulence excited by a random white force.